## How Mg2+ ions lower the SN2@P barrier in enzymatic triphosphate hydrolysis

Van Bochove, Marc A.; Roos, Goedele; Fonseca Guerra, Célia; Hamlin, Trevor A.; Bickelhaupt, F. Matthias

***published in***
Chemical Communications
2018

***DOI (link to publisher)***
10.1039/c8cc00700d

***document version***
Publisher's PDF, also known as Version of record



***citation for published version (APA)***
Van Bochove, M. A., Roos, G., Fonseca Guerra, C., Hamlin, T. A., & Bickelhaupt, F. M. (2018). How $Mg^{2+}$ ions lower the $S_N2$@P barrier in enzymatic triphosphate hydrolysis. *Chemical Communications*, *54*(28), 3448-3451. https://doi.org/10.1039/c8cc00700d

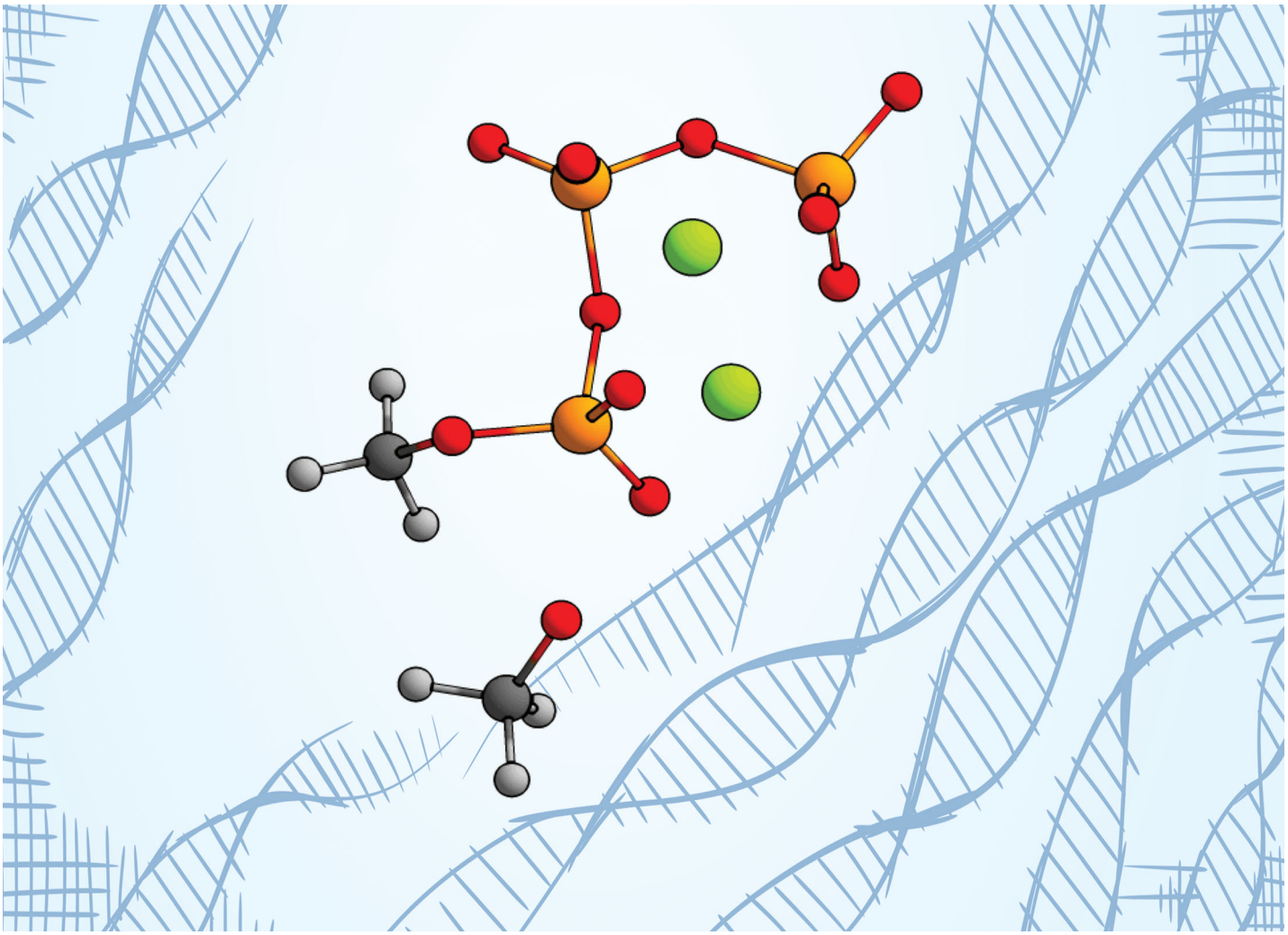

**Showcasing research from the group of Professor Matthias Bickelhaupt at Vrije Universiteit Amsterdam, The Netherlands.**

How $Mg^{2+}$ ions lower the $S_N2$@P barrier in enzymatic triphosphate hydrolysis

This work explores the effects of triphosphate deprotonation and elucidates the physical factors underpinning the enzymatic role of $Mg^{2+}$ ions on this pivotal $S_N2$@P reaction.

## As featured in:


See Trevor A. Hamlin, F. Matthias Bickelhaupt *et al.*, *Chem. Commun.*, 2018, **54**, 3448.

ROYAL SOCIETY OF CHEMISTRY

rsc.li/chemcomm

Registered charity number: 207890

ChemComm

COMMUNICATION

View Article Online
View Journal | View Issue



Cite this: *Chem. Commun.*, 2018, **54**, 3448

Received 26th January 2018,
Accepted 7th March 2018

DOI: 10.1039/c8cc00700d

rsc.li/chemcomm



# How $Mg^{2+}$ ions lower the $S_N2$@P barrier in enzymatic triphosphate hydrolysis†

Marc A. van Bochove,[a] Goedele Roos,[a] Célia Fonseca Guerra,[ab] Trevor A. Hamlin *[a] and F. Matthias Bickelhaupt *[ac]

**Our quantum chemical activation strain analyses demonstrate how $Mg^{2+}$ lowers the barrier of the enzymatic triphosphate hydrolysis through two distinct mechanisms: (a) weakening of the leaving-group bond, thereby decreasing activation strain; and (b) transition state (TS) stabilization through enhanced electrophilicity of the triphosphate PPP substrate, thereby strengthening the interaction with the nucleophile.**

Hydrolysis of phosphate esters, the building blocks of life, is undeniably of significant biological importance. Triphosphate (PPP) hydrolysis is ubiquitous in biochemistry, serving a primary role in DNA and RNA replication, signal, and energy transduction.[1] $Mg^{2+}$ is the most abundant metal ion cofactor in enzymatic systems, with intra-cellular concentrations in the millimolar range.[2] This counter ion plays a pivotal role in enzymatic PPP hydrolysis,[1] speeding up an otherwise exceptionally slow biological reaction.[3] Despite a number of thorough experimental and computational studies, a mechanistic consensus for how these enzymes operate has yet to be resolved.[4]

Herein, we leverage quantum chemical calculations to elucidate the mechanism by which $Mg^{2+}$ ions lower the reaction barrier of PPP hydrolysis, as it occurs in DNA polymerase. In this enzymatic reaction, the fully deprotonated PPP substrate, of which a terminal phosphate group ($P^{\alpha}$) is attacked by a nucleophile, leads to expulsion of the remaining pyrophosphate leaving group (PP) (Scheme 1).[5] Ionization, that is, deprotonation of PPP is shown to increase this $S_N2$@P barrier. This was recently supported for a related and equally important enzymatic reaction involving the hydrolysis of PPP by a water molecule.[6] This particular reaction is a key step in NTPase enzymes and involves attack by water on the $P^{\gamma}$, leading to hydrolysis of PPP into diphosphate and inorganic phosphate.[7] Studies exploring the reaction profile of PPP hydrolysis[8,9] point to the catalytic effect of enzyme residues and to a major effect of $Mg^{2+}$.[1,8,9] $Mg^{2+}$ was shown to have a minimal effect on transition state geometries for this reaction and barriers were highly dependent on the binding mode of the counter ion.[10] The precise mechanism through which $Mg^{2+}$ operates in these $S_N2$@P reactions still requires elucidation despite these insights. To that end, we show, based on sophisticated quantum chemical activation strain analyses,[11] that the $Mg^{2+}$ catalytic effect stems from two distinct mechanisms: (a) weakening of the leaving group bond thereby decreasing activation strain; and (b) transition state (TS) stabilization through enhanced electrophilicity of the PPP substrate, thereby strengthening the interaction with the nucleophile.

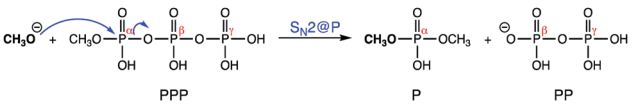


Scheme 1 Model reactions for triphosphate (PPP) hydrolysis *via* $S_N2$@P. The nucleophile is varied between $CH_3O^-$ (shown) and $CH_3OH$, the triphosphate along PPP (shown), $[PPP-H]^-$, $[PPP-2H]^{2-}$ and $[PPP-4H]^{4-}$, and 0–2 $Mg^{2+}$ ions are introduced on various positions.

The existence and height of $S_N2$ barriers is determined by the interplay of steric demand around the electrophilic atom being attacked, the strength of the nucleophile–substrate interaction, as well as solvent effects.[12] In addition, counter ions can significantly affect the $S_N2$ reaction barriers.[13] We have quantum chemically explored and analyzed the $S_N2$@P potential energy surface (PES) for methanol- and methoxide-induced PPP hydrolysis in aqueous solution (Scheme 1) using density functional theory (DFT) at COSMO-ZORA-OLYP/TZ2P as implemented in the ADF program.[14] The OLYP functional reproduces $S_N2$ barriers within a few kcal $mol^{-1}$ compared to high-level

[a] *Department of Theoretical Chemistry and Amsterdam Center for Multiscale Modeling, Vrije Universiteit Amsterdam, De Boelelaan 1083, NL-1081 HV Amsterdam, The Netherlands. E-mail: t.a.hamlin@vu.nl, f.m.bickelhaupt@vu.nl*

[b] *Leiden Institute of Chemistry, Gorlaeus Laboratories, Leiden University, NL-2311 EZ Leiden, The Netherlands*

[c] *Radboud University, Institute for Molecules and Materials, Heyendaalseweg 135, NL-6525 AJ Nijmegen, The Netherlands*

† Electronic supplementary information (ESI) available. See DOI: 10.1039/c8cc00700d

Table 1 Energies relative to reactant complex (in kcal mol$^{-1}$) and overall charge $Q$ (in a.u.) of stationary points for $S_N2$@P reactions in aqueous solution[a]

| No. | Nucleophile | Substrate | $Q$ | RC[a] | TS | PC | P[b] |
|---|---|---|---|---|---|---|---|
| 1a | $CH_3O^-$ | PPP | −1 | 0 (−44.4) | 23.2 | 14.1 | 13.9 |
| 1b | $CH_3OH$ | PPP | 0 | 0 | 25.8 | 7.3 | 10.6 |
| 2a | $CH_3O^-$ | $[PPP–H]^-$ | −2 | 0 | 13.8 | −39.2 | −38.5 |
| 2b | $CH_3OH$ | $[PPP–H]^-$ | −1 | 0 | 24.3 | 15.2 | 14.9 |
| 2c | $CH_3O^-$ | $[PPP–H]^-(Mg^{2+})$ | 0 | 0 | 15.4 | −69.5 | −27.1 |
| 2d | $CH_3OH$ | $[PPP–H]^-(Mg^{2+})$ | +1 | 0 | 22.7 | 1.0 | 26.4 |
| 2e | $CH_3O^-(Mg^{2+})$ | $[PPP–H]^-$ | 0 | 0 (−33.9) | 29.6 | 8.6 | 9.1 |
| 3a | $CH_3O^-$ | $[PPP–2H]^{2-}$ | −3 | 0 | 20.6 | — | −35.0 |
| 3b | $CH_3OH$ | $[PPP–2H]^{2-}$ | −2 | 0 | 28.9 | — | 18.4 |
| 3c | $CH_3O^-$ | $[PPP–2H]^{2-}(Mg^{2+})$ | −1 | 0 | 14.8 | −48.0 | −1.3 |
| 3d | $CH_3OH$ | $[PPP–2H]^{2-}(Mg^{2+})$ | 0 | 0 | 26.1 | 8.3 | 31.7 |
| 3e | $CH_3O^-(Mg^{2+})$ | $[PPP–2H]^{2-}$ | −1 | 0 (−46.0) | 53.6 | −27.3 | −1.9 |
| 4a | $CH_3O^-$ | $[PPP–4H]^{4-}$ | −5 | 0 | 33.1 | — | −19.1 |
| 4b | $CH_3OH$ | $[PPP–4H]^{4-}$ | −4 | 0 | 46.1 | — | 33.2 |
| 4c | $CH_3O^-$ | $[PPP–4H]^{4-}(Mg^{2+})$ | −3 | 0 | 22.4 | −32.6 | −6.5 |
| 4d | $CH_3OH$ | $[PPP–4H]^{4-}(Mg^{2+})$ | −2 | 0 (−0.9) | 35.1 | 17.6 | 40.8 |
| 4e | $CH_3O^-(Mg^{2+})$ | $[PPP–4H]^{4-}$ | −3 | 0 (−52.9) | 51.8 | −43.0 | −16.9 |
| 4f[c] | $CH_3O^-$ | $[PPP–4H]^{4-}(Mg^{2+})_2$ | −1 | 0 | 11.7 | −61.9 | −14.6 |
| 4fb[c] | $CH_3O^-$ | $[PPP–4H]^{4-}(Mg^{2+})_2$ | −1 | 0 | 9.9 | −63.7 | −16.4 |
| 4g | $CH_3OH$ | $[PPP–4H]^{4-}(Mg^{2+})_2$ | 0 | 0 | 21.0 | 3.8 | 37.1 |
| 4h | $CH_3O^-(Mg^{2+})$ | $[PPP–4H]^{4-}(Mg^{2+})$ | −1 | 0 (−35.9) | 44.2 | 15.3 | 35.9 |

[a] Computed at COSMO-ZORA-OLYP/TZ2P. If RC exists: stabilization of RC relative to separate reactants, $E$(RC) − $E$(R), in parentheses. [b] In reactions involving $Mg^{2+}$ ions, the products P are calculated based on chelation of the $Mg^{2+}$ to pyrophosphate leaving group. [c] Substrate is **4R″** in reaction 4f and **4R″(2)** in reaction 4fb (see Scheme S1, ESI).

*ab initio* benchmarks.[14c] The computed trends in reactivity for our simple model systems, which are sufficiently generic to be applied to other biologically related processes, are in good agreement with experimental hydrolysis studies.[15] Full numerical details can be found in Tables S1–S4 (ESI†) along with detailed information on the effect of introducing discrete water molecules coordinating to $Mg^{2+}$ counter ions.

We first examine the effect on the $S_N2$@P mechanism of varying the extent of deprotonation in model reactions 1–4 (Table 1) along which we remove either no protons (neutral PPP), the β-proton ($[PPP–H]^-$), the α- and γ-protons ($[PPP–2H]^{2-}$), or the α-, β- and γ-protons ($[PPP–4H]^{4-}$). This order of deprotonation reflects the lowest energy isomer for each deprotonation.

We then examine the effect of introducing 0–2 $Mg^{2+}$ counter ions (reaction sub-numbering a–h) on various positions, including both the nucleophile and PPP, which mimic the $Mg^{2+}$ positions in the reported crystal structure of DNA polymerase.[16] Our computed barriers and reaction energies relative to reactants or – if present – reactant complexes (RC) are collected in Table 1 and selected stationary structures are shown in Fig. 1.

Nucleophilic attack by $CH_3O^-$ at neutral PPP (reaction 1a) resembles archetypal model reactions of the type $X^-$ + $(MeO)_3P–Y$.[12c–e] Our explorations, however, reveal that this particular reaction system does not constitute a viable biochemical pathway. The PPP hydrolysis reaction has to compete with proton transfer from the α-proton to the nucleophile under formation of a methanol reactant complex (RC) at −44.0 kcal mol$^{-1}$. A central barrier of 23.2 kcal mol$^{-1}$ (Table 1) separates this RC from a very loosely hydrogen-bonded product complex (PC, see Fig. 1). The alcoholic hydrogen is not returned to the phosphate–oxygen during the process, a step that, with a barrier of approximately 40.0 kcal mol$^{-1}$, is far less favorable than the breaking of the $P^{\alpha}$–$O^{\alpha}$ bond. Reaction 1b, in which the same substrate is attacked by methanol, no proton-transfer occurs and the $P^{\alpha}$ is directly attacked resulting in a structurally similar, but more strongly bound PC. The reaction barrier of 25.8 kcal mol$^{-1}$ is slightly higher in the overall endothermic reaction 1b than in reaction 1a. In transition state **1bTS**, the α-proton does play an important role. It transfers to the negatively charged leaving group as the PC is formed and in this way avoids an energetically unfavorable charge separation.

Deprotonation of the PPP substrate suppresses the above-mentioned proton transfer to the nucleophile already upon dissociation of the β-proton, as we go from **1R** (fully protonated PPP) to **2R** (β-proton removed, see Fig. 1). Instead, the nucleophile and substrate are structurally well configured to proceed through the prototypical backside $S_N2$@P pathway. This remains the case also if the α-proton and the γ-proton are dissociated as we go from substrate **2R** to **3R** (α- and γ-protons removed) to **4R** (α-, β- and γ-protons removed), the form in which PPP occurs under physiological conditions.[1c]

Stepwise deprotonation of the PPP substrate along **1R**, **2R**, **3R** and **4R** furthermore causes reaction barriers for both, $CH_3O^-$ and $CH_3OH$-induced $S_N2$@P reactions, to first decrease when going from the neutral substrate **1R** (reactions 1a and 1b) to the negatively charged substrate **2R** (reactions 2a and 2b), and then to increase as the extent of triphosphate ionization further increases in **3R** and **4R** (reactions 3a, 3b, 4a and 4b). For example, along the reactions 1a, 2a, 3a and 4a, which involve the nucleophilic attack by $CH_3O^-$, the reaction barrier goes

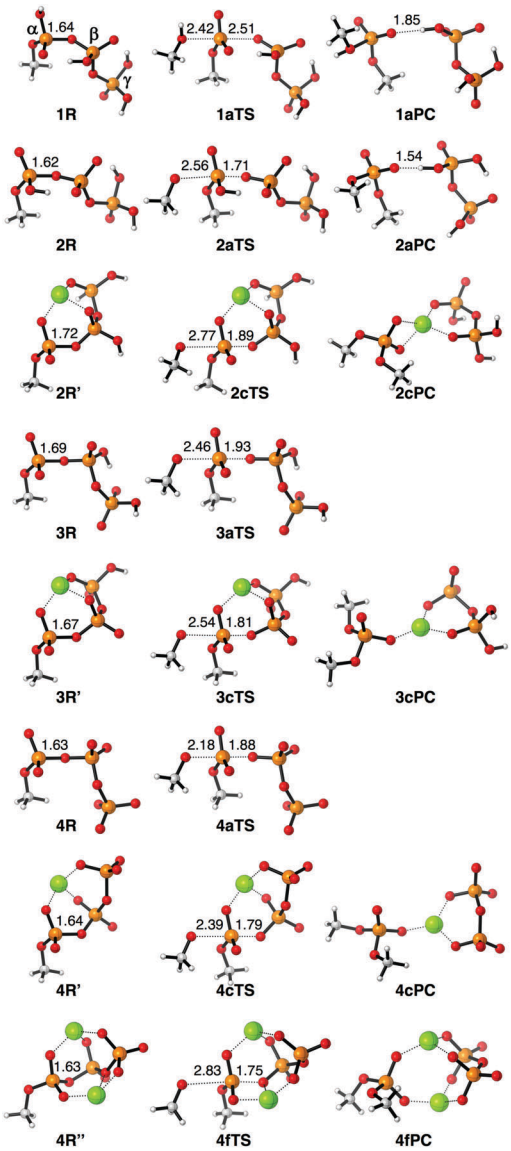


Fig. 1 Structures of selected stationary points (in Å) along $S_N2$@P reactions in aqueous solution, computed at COSMO-ZORA-OLYP/TZ2P (C = silver, H = white, O = red, P = orange, Mg = green; indicated Mg–O contacts are 1.9–2.1 Å).

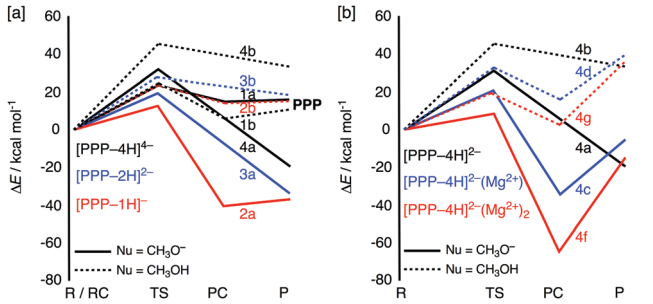


Fig. 2 Reaction profiles for model $S_N2$@P reactions in aqueous solution, computed at COSMO-ZORA-OLYP/TZ2P: [a] $CH_3O^-$ or $CH_3OH$ + PPP, $[PPP–H]^-$, $[PPP–2H]^{2-}$ and $[PPP–4H]^{4-}$. [b] $CH_3O^-$ or $CH_3OH$ + $[PPP–4H]^{4-}$, $[PPP–4H]^{4-}(Mg^{2+})$ and $[PPP–4H]^{4-}(Mg^{2+})_2$.

from 23.2 to 13.8 to 20.6 to 33.1 kcal $mol^{-1}$ (see Table 1 and Fig. 2a). Reaction barriers are consistently higher in the case of nucleophilic attack by $CH_3OH$ (see reactions 1b, 2b, 3b, 4b in Table 1). In none of the $CH_3OH$-induced reactions does the alcoholic proton transfer to an α-oxygen of PPP. Instead, this proton enters into a $CH_3OH\cdots{}^-O^{\alpha}$ hydrogen bond. This finding is in accordance with a mechanism for catalyzed PPP hydrolysis, in which an enzymatic environment is required to assist deprotonation of the alcoholic oxygen.[1,8,9] Only thereafter, can the resulting alkoxide induce hydrolysis *via* $S_N2$@P with a sufficiently low activation barrier.

Introducing a single $Mg^{2+}$ counter ion to a partially or completely deprotonated PPP yields a complex in which the $Mg^{2+}$ interacts simultaneously with an oxygen of each of the three phosphate moieties (see **2R′**, **3R′** and **4R′** in Fig. 1). The presence of the $Mg^{2+}$ ion significantly lowers all $S_N2$@P reaction barriers (see Fig. 2b). This agrees well with the experimental observation that enzymatic PPP hydrolysis only proceeds if $Mg^{2+}$ ions are present in the reaction mixture.[1b,3] After the TS, $Mg^{2+}$ moves in between the product molecule and the leaving group (see **2cPC**, **3cPC** and **4cPC** in Fig. 1). In the polymerase, it is likely that this stable PC is bypassed completely during the recycling of the $Mg^{2+}$ ions. Our simplified model system does not account for key residues in the active site that would stabilize and retain $Mg^{2+}$ and, therefore, it is thermodynamically favorable for $Mg^{2+}$ to leave with the leaving PP.

Addition of a second $Mg^{2+}$ to the fully deprotonated PPP lowers the barrier for the backside $S_N2$@P reaction even further and furnishes feasible reaction channels. The most stable structure in the case of two $Mg^{2+}$ ions interacting with PPP, *i.e.*, **4R″**, occurs when one $Mg^{2+}$ interacts with an oxygen of each phosphate and the other $Mg^{2+}$ interacts with a different α- and γ-oxygen plus the oxygen connecting the β- and γ-phosphate (Scheme S1, ESI†). Nucleophilic attack by $CH_3O^-$ at **4R″** now leads to $S_N2$@P substitution and PPP hydrolysis *via* a barrier of only 11.7 kcal $mol^{-1}$ (reaction 4f, Table 1). A slightly more favorable $S_N2$@P pathway exists which proceeds *via* initial dissociation of the coordination bond in **2R″** between $Mg^{2+}$ and the oxygen connecting the β- and γ-phosphate, leading to **4R″(2)** (Scheme S1, ESI†). This isomerization proceeds with a barrier of 1.9 kcal $mol^{-1}$ and is slightly endothermic by just 1.8 kcal $mol^{-1}$. From here, the $S_N2$@P barrier for the $CH_3O^-$ nucleophile is merely 9.9 kcal $mol^{-1}$ (reaction 4fb, see Table 1).

In the case that an $Mg^{2+}$ ion coordinates to the nucleophile $CH_3O^-$ on its path towards the α-phosphorus, the $S_N2$@P reaction barriers are raised to the extent that the pathway becomes unviable (reactions 4e and 4h, see Table 1). One reason is that $CH_3O^-$ deviates from its path for backside attack as it moves along with its $Mg^{2+}$ to form a highly stabilized RC (by −52.9 and −35.9 kcal $mol^{-1}$ for reactions 4e and 4h, respectively) in which the metal cation interacts with two oxygens on the α-phosphate group. Both, the energetic penalty associated with breaking this stable interaction in the RC as well as the reduced intrinsic nucleophilicity of $CH_3O^-(Mg^{2+})$[13] relative to $CH_3O^-$, lead to prohibitively high barriers of

 

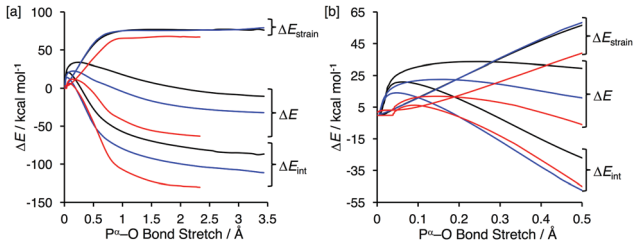


Fig. 3 [a] Activation strain analyses for $S_N2$@P reactions 4a ($CH_3O^-$ + $[PPP-4H]^{4-}$, black), 4c ($CH_3O^-$ + $[PPP-4H]^{4-}(Mg^{2+})$, blue), and 4f ($CH_3O^-$ + $[PPP-4H]^{4-}(Mg^{2+})_2$, red) and [b] activation strain diagram focusing on the region surrounding the transition state.

51.8 and 44.2 kcal mol$^{-1}$ for reactions 4e and 4h, respectively (see Table 1). In order to reveal the physical factor behind the catalytic effect of $Mg^{2+}$ on the $S_N2$@P reactions, we next performed activation strain analyses[11] for reactions 4a, 4c and 4f, which go with 0, 1 and 2 $Mg^{2+}$ ions and barriers of 33.1, 22.4 and 11.7 kcal mol$^{-1}$.

The resulting activation strain diagrams, in Fig. 3a, decompose the reaction potential energy surface $\Delta E$ into the strain $\Delta E_{strain}$ of the distorting reactants plus the interaction $\Delta E_{int}$ between these reactants, along the reaction coordinate defined as the breaking of the $P^{\alpha}$–$O^{\alpha}$ bond. As explained below, we find that $Mg^{2+}$ lowers the barrier of the enzymatic PPP hydrolysis through two distinct mechanisms: (a) weakening the leaving-group bond thereby decreasing activation strain; and (b) transition state (TS) stabilization through enhancement of the TS interaction with the nucleophile (Fig. 3).

Thus, the activation strain diagram in the TS region (see zoom-in, in Fig. 3b) reveals that introducing a single $Mg^{2+}$ ion (blue curve), that is, going from reaction 4a to 4c, enhances the interaction $\Delta E_{int}$ between the incoming $CH_3O^-$ nucleophile, thereby decreasing the barrier by 10.7 kcal mol$^{-1}$. The enhanced interaction is ascribed to a more favorable electrostatic and orbital interaction, as $Mg^{2+}$ reduces the net negative charge (by 4 a.u. upon introducing two $Mg^{2+}$) and lowers the LUMO energy of the substrate (by 1.9 eV upon introducing two $Mg^{2+}$). Thus, coordinating magnesium ions at PPP enhances the electrophilicity of the substrate. However, this single $Mg^{2+}$ has yet no effect on the strain curve $\Delta E_{strain}$. Incorporation of a second $Mg^{2+}$ ion is found to stabilize both, the $\Delta E_{int}$ and $\Delta E_{strain}$ curves, and results in a barrier of only 11.7 kcal mol$^{-1}$, that is, 21.4 kcal mol$^{-1}$ lower than the uncatalyzed process 4a.

The origin for reduced strain in the case of reaction 4f is that the second $Mg^{2+}$ coordinates preferentially to the oxygen atom of the $P^{\alpha}$–$O^{\alpha}$ leaving-group bond in $[PPP-4H]^{4-}$ and effectively stabilizes the evolving net negative charge on the $O^{\alpha}$ atom in the PP leaving group. Thus, as this stabilization increases as the reaction proceeds towards the products, it essentially weakens the leaving-group bond and results in a decrease in the activation strain (see Fig. S1 for details, ESI†).

We thank the Netherlands Organization for Scientific Research (NWO), the PEPSci program, the Dutch Astrochemistry Network, and the NRSC-C for financial support.

## Conflicts of interest

There are no conflicts to declare.

## Notes and references

1 (*a*) T. Nakamura, Y. Zhao, Y. Yamagata, Y.-j. Hua and W. Yang, *Nature*, 2012, **487**, 196–201; (*b*) E. M. De La Cruz and E. M. Ostap, *Methods Enzymol.*, 2009, **455**, 157–192; (*c*) A. J. Berdis, *Chem. Rev.*, 2009, **109**, 2862–2979; (*d*) W. W. Cleland and A. C. Hengge, *Chem. Rev.*, 2006, **106**, 3252–3278; (*e*) L. Stryer, in *Biochemistry*, ed. W. H. Freeman, Company, New York, 1988; (*f*) F. H. Westheimer, *Science*, 1987, **235**, 1173–1178.
2 C. Sissi and M. Palumbo, *Nucleic Acids Res.*, 2009, **37**, 702–711.
3 (*a*) G. K. Schroeder, C. Lad, P. Wyman, N. H. Williams and R. Wolfenden, *Proc. Natl. Acad. Sci. U. S. A.*, 2006, **103**, 4052–4055; (*b*) C. Lad, N. H. Williams and R. Wolfenden, *Proc. Natl. Acad. Sci. U. S. A.*, 2003, **100**, 5607–5610.
4 (*a*) H. A. Hassan, S. Rani, T. Fatima, F. A. Kiani and S. Fischer, *Biophys. Chem.*, 2017, **230**, 27–35; (*b*) F. Duarte, A. Barrozo, J. Åqvist, N. H. Williams and S. C. L. Kamerlin, *J. Am. Chem. Soc.*, 2016, **138**, 10664–10673; (*c*) M. G. Khrenova, B. L. Grigorenko, A. B. Kolomeisky and A. V. Nemukhin, *J. Phys. Chem. B*, 2015, **119**, 12838–12845; (*d*) W. Li, T. Rudack, K. Gerwert, F. Gräter and J. Schlitter, *J. Chem. Theory Comput.*, 2012, **8**, 2596–3604; (*e*) C. Biertümpfel, Y. Zhao, Y. Kondo, S. Ramón-Maiques, M. Gregory, J. Y. Lee, C. Masutani, A. R. Lehmann, F. Hanaka and W. Yang, *Nature*, 2010, **465**, 1044–1048; (*f*) D. Herschleg and W. P. Jencks, *J. Am. Chem. Soc.*, 1989, **111**, 7587–7596.
5 C. A. Brautigm and T. A. Steitz, *Curr. Opin. Struct. Biol.*, 1998, **8**, 54–63.
6 F. A. Kiani and S. Fischer, *BMC Biochem.*, 2016, **17**, 12.
7 D. R. Trentham, J. F. Eccleston and C. R. Bagshaw, *Rev. Biophys.*, 1976, **9**, 217.
8 See, for example: (*a*) B. R. Prasad, N. V. Plotnikov, J. Lameira and A. Warshel, *Proc. Natl. Acad. Sci. U. S. A.*, 2013, **110**, 20509–20514; (*b*) V. A. Mironov, M. G. Khrenova, L. A. Lychko and A. V. Nemukhin, *Proteins*, 2015, **83**, 1046–1053; (*c*) L. Perea, B. D. Freudenthal, W. A. Beard, D. D. Shock, L. G. Pedersen and S. H. Wilson, *Proc. Natl. Acad. Sci. U. S. A.*, 2015, **112**, E5228–E5236.
9 (*a*) Q. Lu, N. Nassar and J. Wang, *Chem. Phys. Lett.*, 2011, **516**, 233–238; (*b*) C. F. Matta, A. A. Arabi and T. A. Keith, *J. Phys. Chem. A*, 2007, **111**, 8864–8872; (*c*) Y. N. Wang, I. A. Topol, J. R. Collins and S. K. Burt, *J. Am. Chem. Soc.*, 2003, **125**, 13265–13273.
10 A. Barrozo, D. Blaha-Nelson, N. H. Williams and S. C. L. Kamerlin, *Pure Appl. Chem.*, 2017, **89**, 715–727.
11 (*a*) F. M. Bickelhaupt and K. N. Houk, *Angew. Chem., Int. Ed.*, 2017, **56**, 10070–10086; (*b*) L. P. Wolters and F. M. Bickelhaupt, *WIREs Comput. Mol. Sci.*, 2015, **5**, 324–343; (*c*) I. Fernandez and F. M. Bickelhaupt, *Chem. Soc. Rev.*, 2014, **43**, 4953–4967; (*d*) D. H. Ess and K. N. Houk, *J. Am. Chem. Soc.*, 2007, **129**, 10646–10647.
12 (*a*) T. A. Hamlin, M. Swart and F. M. Bickelhaupt, *ChemPhysChem*, 2018, **19**, DOI: 10.1002/cph.201701363; (*b*) T. A. Hamlin, B. van Beek, L. P. Wolters and F. M. Bickelhaupt, *Chem. – Eur. J.*, 2018, **24**, DOI: 10.1002/chem.201706075; (*c*) S. C. A. H. Pierrefixe, S. J. M. van Stralen, J. N. P. van Stralen, C. Fonseca Guerra and F. M. Bickelhaupt, *Angew. Chem., Int. Ed.*, 2009, **48**, 6469–6471; (*d*) M. A. van Bochove and F. M. Bickelhaupt, *Eur. J. Org. Chem.*, 2008, 649–654; (*e*) M. A. van Bochove, M. Swart and F. M. Bickelhaupt, *J. Am. Chem. Soc.*, 2006, **128**, 10738–10744; (*f*) M. A. van Bochove, M. Swart and F. M. Bickelhaupt, *Phys. Chem. Chem. Phys.*, 2009, **11**, 259–267.
13 J. Z. A. Laloo, L. Rhyman, P. Ramasami, F. M. Bickelhaupt and A. de Cozar, *Chem. – Eur. J.*, 2016, **22**, 4431–4439.
14 (*a*) G. te Velde, F. M. Bickelhaupt, E. J. Baerends, C. Fonseca Guerra, S. J. A. van Gisbergen, J. G. Snijders and T. Ziegler, *J. Comput. Chem.*, 2001, **22**, 931–967; (*b*) For COSMO, see: A. Klamt and G. Schüürmann, *J. Chem. Soc., Perkin Trans. 2*, 1993, 799–805; (*c*) For performance analyses, see: M. Swart, M. Solà and F. M. Bickelhaupt, *J. Comput. Chem.*, 2007, **28**, 1551–1560.
15 R. Ramirez, J. F. Marecek and J. Szamosi, *J. Org. Chem.*, 1980, **45**, 4748–4752.
16 V. K. Batra, W. A. Beard, D. D. Shock, J. M. Krahn, L. C. Pedersen and S. H. Wilson, *Structure*, 2006, **14**, 757–766.